Final submitted version of
Gabbud, C. Micheletti, N. and Lane, S.N., 2016. Response of a temperate Alpine valley glacier to climate change at the decadal scale. Geografiska Annaler A: Physical Geography, 98, 81–95.
https://onlinelibrary.wiley.com/doi/full/10.1111/geoa.12124?scrollTo=references

RESPONSE OF A TEMPERATE ALPINE VALLEY GLACIER TO CLIMATE CHANGE AT THE DECADAL SCALE

GABBUD, Chrystelle, MICHELETTI, Natan and LANE, Stuart N.

Institute of Earth Surface Dynamics (IDYST), University of Lausanne, Lausanne, Switzerland

Abstract

Glacier advance and recession are considered as key indicators of climate change. Understanding the relationship between climatic variations and glacial responses is crucial. Here, we apply archival digital photogrammetry to reconstruct the decadal scale glacial history of an unmonitored Alpine valley glacier, the Haut Glacier d'Arolla, Switzerland, and we use the data generated to explore the linkages between glacier recession and climate forcing. High precision Digital Elevation Models (DEMs) were derived. They show continual recession of the glacier since 1967, associated with long-term climatic amelioration but only a weak reaction to shorter-term climatic deterioration. Glacier surface velocity estimates obtained using surface particle tracking showed that, unlike for most Swiss glaciers during the late 1970s and early 1980s, ice mass flux from the accumulation zone was too low to compensate for the effects of glacier thinning and subsequent snout recession, especially during the rapid warming that occurred through the 1980s. The results emphasise the dangers of inferring glacier response to climate forcing from measurements of the terminus position only and the importance of using remote sensing methods as an alternative, especially where historical imagery is available.

Key words

Glacier recession, Climate change, archival digital photogrammetry, Orthoimagery, Digital Elevation Model (DEM), Haut Glacier d'Arolla, Remote Sensing

Introduction

Glacier advance and recession are considered as key indicators of climate change (e.g. Houghton *et al*. 1996). Unlike a weather station, which measures the temporal variability of individual variables, glaciers integrate climatic variability, as a function of a glacier's response time, manifest as variations in length, surface, volume, thickness or flow rate (Francou and Vincent 2010). Measuring their change can provide very valuable data on how the cryosphere is responding to the integrated effects of a range of changing climatic parameters, independent of short-term variability. It may be achieved either by direct measurement, such as annual measurement of snout position (e.g. Purdie *et al*. 2014) or indirect monitoring, the latter often using remote sensing. Annual measurement of snout position may yield general trends in glacier response to climate forcing but the results obtained will be complicated because snout position is not only a function of annual glacier mass balance, but also the speed of ice flow from the accumulation zone to the ablation zone, and hence glacier thickness, valley slope and glacier hypsometry. Thus the scales of climate variability recorded in a snout record will vary between glaciers. Those that react more quickly will contain a greater range of scales than those that react more slowly. This is why the notion of glacier reaction time (e.g. Oerlemans 2001; Winkler and Nesje 2009) may be of more value than glacier response time in considering glacier response to changing climate. Response time is the time require for a glacier to evolve to a new state of equilibrium after a given change in mass balance and hence in climate (Johannesson *et al*. 1989). If climate is changing continuously over a number of different time scales, it is unlikely that the glacier ever reaches equilibrium. Whilst this does not prevent the use of the response time in glacier comparison, the reaction time may be of more use in global change studies as the reaction time will define the scales of climate variability that will be seen in glacier snout position. The reaction time is the time between a given change in climate that can result in a change in glacier mass balance, and the time of first response of the glacier terminus to this change (Oerlemans, 2001). As Winkler and Nesje (2009) conclude, there is an urgent need for comparative studies of how glacier snouts respond to short-term and (comparatively) extremely rapid climate change such that the inference of climate change impacts on glacier recession is correct. In turn, this requires measurement of more than just snout position through time.

Remote sensing has the advantage that it potentially provides data on entire ice sheets and glaciers. For smaller valley-based glaciers, remote sensing methods need higher ground resolutions, of the order of metres rather than 10s of metres. They are particularly powerful when historical images are available that can be used to reconstruct systems that have not been measured directly. Photogrammetry, a science initially motivated by the quantification of glacier recession from photographs (Finsterwalder 1890), has proved to be valuable in this respect (e.g. Small *et al.* 1984; Brecher 1986; Hubbard *et al.* 2000; Baltsavias *et al.* 2001; Kääb 2001; Keutterling and Thomas 2006; Barrand *et al.* 2009; Heid and Kääb 2012).

The main aim of this paper is to apply digital photogrammetry to historical images (archival digital photogrammetry) to an Alpine valley glacier with no established advance/retreat history (the Haut Glacier d'Arolla, Switzerland) and to use the data generated to explore the linkages between glacier terminus recession and climate forcing at the decadal scale. The specific objectives are: (1) to generate high resolution and precise DEMs from historical digital imagery for the period 1967 to present; (2) to orthorectify the imagery to correct for distortion and relief effects; (3) to use the DEM differences to determine surface lowering; (4) to combine these data with ice discharge estimates to estimate volume loss; and (5) to identify the climate forcing associated with the changes and their impacts upon water yield. The results allow two conclusions to be reached. First, provided that the aerial imagery available has sufficient scale and that it is possible to trace surface features to get the estimate of surface velocity needed to get ice flux, it is possible to calculate rates of volume loss/gain. Second, the case study illustrates the difficulty of inferring sub-decadal scale to decadal climate forcing of valley glaciers from measurements of the position of the snout terminus.

Climate Change and glaciers in a Swiss context

It is well-established that glaciers are subject to climate changes, which result from all climate parameters, but especially temperature and precipitation. The response of glaciers is to change the amount and the spatial distribution of mass accumulation and melt by ablation (Hooke 2005). Global climate is rapidly changing and Switzerland has been particularly affected. Since the beginning of the measurements in 1864, which is also generally taken as the end of the Little Ice Age in Switzerland, average temperature has increased by approximately 0.12 °C per decade, an increase of 1.7 °C over the period 1864-2011 (OFEV and MétéoSuisse 2013). Although this trend has been punctuated by periods of general cooling, all annual means since the mid-1980s have remained above the reference mean (Figure 1) (MétéoSuisse 2010. Bulletin climatologique annuel – rétrospective annuelle 2009, available at:http://www.meteosuisse.admin.ch/web/fr/climat/climat_aujourdhui/retrospective_annuelle/flash2009.html (Viewed on the 01.07.2014)).

This study spans two main climatic periods: (1) between the 1960s and the early 1980s, a relatively cooler period occurred following a warmer period in the 1950s; and (2) a much warmer period from the mid-1980s which has been maintained until present although the rate of rise slowed from the late 1990s onwards. Temperature records since the Little Ice Age showed 1994 as the hottest year on record, followed by 2003 and 2002. Unlike for temperature, there is no general trend in Switzerland in terms of precipitation, although local trends may be found in individual stations. For high altitude areas (> 2500 m a.s.l.), the impacts of climate change on snow cover appear to be negligible (ONERC 2008). Sunshine duration decreased significantly between the 1960s and the 1980s, before rising again since (OFEV and MétéoSuisse 2013).

Globally, similar sorts of changes have been associated with the reduction in the extent of snow and ice masses (IPCC 2008). Glaciers have been reported to be in a general state of negative mass balance, and also in a state of retreat (IPCC 2013). For instance, in Switzerland, almost one third of the total glacierized area has disappeared since 1973 (Fischer *et al*. 2014). Given the lack of a clear snowfall trend at the altitudes typical of Swiss glaciers, but a clear annual warming trend, it is probable that the recession is an ablation signal, related both to a progressive increase in duration of the melt season and warmer temperatures within that season (OcCC and ProClim 2007). Progressive loss of ice may cause a catchment to switch from a glacial regime, where melt is dominant in the period July through to September, to a nival-glacial regime where there is greater proportionate contribution from snow melt, that occurs in spring as well as summer, and where the reduced glacier stock makes water yield more dependent upon interannual variability in snow fall (OcCC and ProClim 2007).

Methodology

Study site

The catchment of the Haut Glacier d'Arolla (Figure 2a) is located at the head of the Val d'Hérens, Valais, in the Swiss Alps. This temperate glacier measured 3.46 km^2 in 2010 (Fischer *et al*. 2014). Its accumulation lies between the top of the Grande Arête to the north (3355 m a.s.l.), the Mont Brûlé to the south (3578 m a.s.l.) and l'Evêque to the west (3232 m a.s.l.). The terminus is at 2579 m a.s.l. and its mean elevation is 2987 m a.s.l. (Fischer *et al*. 2014). Its average surface slope is relatively flat at 16.9° and its aspect is north to north-west in the ablation zone. The glacier lies primarily on a bed of unconsolidated sediments with some bedrock outcrops (Hubbard and Nienow 1997). The Haut Glacier d'Arolla is the source of the river Borgne d'Arolla whose water flows are exploited by HYDRO Exploitation SA (See http://www.hydro-exploitation.ch/ for further information). The climate in the area is temperate, with warm summers, and cold, fairly wet winters, although this general pattern is strongly affected by local relief (Arnold 2005).

This area has been the subject of numerous scientific publications that have, together, changed our understanding of glacier dynamics and subglacial hydrology (e.g. Sharp *et al*. 1993; Harbor *et al*. 1997; Nienow *et al*. 1998; Swift *et al.* 2002; Mair *et al*. 2003; Willis *et al*. 2003; Nienow *et al*. 2005; Fischer *et al*. 2011) and the relationship between glaciers and climate (e.g. Brock *et al*. 2000; Arnold 2005; Pellicciotti *et al*. 2005; Brock *et al*. 2006; Dadic *et al*. 2010). However, there has been almost no attempt to reconstruct the history of glacier recession over recent decades and to identify linkages between this understanding and glacier response over longer time periods.

Contextual data

Micheletti *et al.* (2015) have recently undertaken an assimilation of climate data for the region and this study provided the climate data provided in this paper. Although shorter records were available from closer stations (e.g. Evolène, 9 km from the glacier at an elevation of 1826 m a.s.l.), the data are available only from the 1980s. Instead, we used data from the Swiss NBCN (National Basic Climatological Network) which includes 29 temperature and 46 rainfall measurement stations. For temperature (Figure 2a), we used data from the Col du Grand-Saint-Bernard (GSB) at an altitude of 2461 m a.s.l. and 30 km to the West of the glacier provided by the Swiss Federal Office of Meteorology and Climatology MétéoSuisse. The altitude of this measurement site is similar to the snout of the Haut Glacier d'Arolla. Reflecting Figure 1, Figure 2a shows that mean annual temperatures were generally depressed from the 1950s to the early 1980s, encompassing the first part of this study, but rose rapidly between the mid 1980s and the early 1990s. Precipitation is a little more complicated as the Col du Grand-Saint-Bernard is more strongly affected by southerly rain bearing systems than Arolla and so has higher annual rainfall totals. Correlation with shorter-term records for the village of Arolla suggested that the record of Hérémence (altitude 1210 m.a.s.l), to the North of Arolla, was more reliable and so the Hérémence data were used in this study. It should be noted that for rainfall, the absolute rainfall totals may not be reliable but that the patterns will be acceptable. So, following Micheletti *et al.* (2015) we used the Hérémence record. Figure 2b suggests substantial inter annual variability in precipitation totals, but with a 5 year running mean, some systematic variability superimposed on rising annual precipitation to around 2000. Simulations of snow cover by Micheletti *et al.* (2015) in an adjacent basin, at similar altitudes, suggests that the wetter period that starts in the late 1970s (Figure 2b) was sufficient to depress likely equilibrium line altitudes until the rapid warming in the mid 1980s. This was not the case for the wetter period from the early 1990s to early 2000s, attributed to the generally warmer mean annual temperatures (Figure 2b). In addition, hourly river discharge data for the Haut Glacier d'Arolla were obtained from HYDRO Exploitation SA from 1962.

Digital Elevation Models and production of orthoimagery

Archival digital photogrammetry was used to construct Digital Elevation Models (DEMs) from historical aerial imagery. Digital photogrammetry is well-established for glacier monitoring (e.g. Pellikka and Rees 2010), mass balance determination (e.g. Baltsavias *et al*. 2001; Hubbard *et al*. 2000; Huss *et al*. 2010) and computation of the volumes of ice mass change (e.g. Keutterling and Thomas 2006; Barrand *et al*. 2009). The aerial imagery was provided by the Swiss Federal Office of Topography (Swisstopo), with scales varying between 1:9,000 and 1:25,000. The aerial imagery was scanned from diapositives by Swisstopo to photogrammetric standard at a resolution of 14 μm (1814 dpi). All images were obtained during the months of August and September for: 1967, 1977, 1983, 1988, 1997, 2000, 2005 and 2009. This provides a 42 year record of glacial history for the catchment. Table 1 shows the theoretical precision (*p*) of elevations that might be obtained with these aerial images (after Lane *et al.* 2010) given their scale (1:*s*, where s is the flying height divided by the focal length of the sensor used to acquire the imagery) and the scanning resolution (*r*) used. Following Lane *et al.* (2010):

$$\pm p = r\, s$$

$$R \approx 5\, p$$

[1a and 1b]

where *R* is the best available spatial resolution of derived elevations.

Application of digital photogrammetry required ground control points (GCPs) to be visible on the aerial images used for DEM determination. However, as this study uses historical aerial imagery obtained for other purposes, GCPs were not available. Thus, archival digital photogrammetric methods were applied (e.g. Chandler 1999; Lane *et al.* 2010). These use points that can be confidently identified as stable over the timescale of the study, in a two step process: (1) the positions of such points were obtained with differential GPS (dGPS); and (2) these were mapped onto 0.5 m orthoimagery, provided by Swisstopo for 2004, to check that they were located within generally stable zones. The dGPS data were obtained by Leica SR530 and Trimble R10 GNSS/GPS/Glonass systems using the Real-Time Kinematic (RTK) method. Measurements were made with reference to a fixed and continually logging base station. The co-ordinates of the latter were post-processed using the Swiss AGNES network of continually recording dGPS stations and transformed into the Swiss coordinate system CH1903+. All GCPs measured for the photogrammetry were then post-processed to this base station. A total of 51 GCPs were mapped initially and of these about 20 were deemed to be identifiable and stable (lateral displacements of < ±0.3 m, that is commensurate with image resolution). However, these were not uniformly distributed in space, because of constraints associated with access to certain parts of the basin and because much of the basin contained unstable ground (e.g. ice cored moraine).

All the computational operations were performed in the Leica Photogrammetry Suite of ERDAS IMAGINE® 2008. Camera Calibration Certificates provided by Swisstopo were used to remove lens distortion and to establish the interior geometry of the aerial images (the principal points of autocollimation (PPA) and symmetry (PPS), the focal length and the fiducial marks). The exterior orientation (i.e. the positional elements X_0, Y_0, Z_0 and the angular and rotational elements ω (around the X axis), ϕ (around the Y axis) and κ (around the Z axis)) were determined in a simultaneous bundle adjustment using the field-measured dGCPs. Automatic generation of tie points was used to improve the precision of the bundle adjustment, with the objective that the root mean square error (RMSE) of the solution (i.e. the fit of the solution) was commensurate with the theoretical precision (as defined by the image scale and the scanning resolution, Table 1). Tie points are particularly important where the availability of ground control is limited or constrained spatially. By measuring the position of a point on two images, four measurements (two sets of (x, y) image co-ordinates) are obtained. By doing so, for a data point with only three unknowns (X, Y and Z) there is a net gain of one measurement. Thus, tie points can improve the quality of the solution. If the RMSE of the solution is commensurate with the theoretical precision, then the solution will provide data of a quality that is commensurate with the scale of the imagery.

Once an acceptable bundle adjustment had been obtained for each image date, real-world coordinate 3D data were extracted using stereo-matching. The automated terrain extraction parameters used were those advised for mountainous regions (ERDAS 2009).

Each pair of aerial images was used to create a Digital Elevation Model (DEM) and a relief shaded model, in the software ArcGIS. DEMs were derived in raster form, each in the same collocated X Y grid, with a 1 m resolution. These results were then used to orthorectify the raw aerial images to a 0.3 m resolution. The orthoimages, aided by the relief-shaded model, were manually digitised in ESRI ArcGIS to identify the glacier margin for each date. As snow cover prevented data acquisition on the upper part of the glacier, an upstream boundary common to all dates was chosen, downstream of which data could be reliably used. This meant that the focus of the work was upon recession of the glacier snout.

DEMs of difference were calculated for time-consecutive DEMs for the part of the glacier that was ice covered in all aerial images. Volumes of ice mass gain/loss were extracted for consecutive time periods from the DEMs of difference, constraining each by the digitised outline for the start of each time period.

Management of error and determination of data uncertainty

During each of the above stages, attempts were made both to minimize error and to quantify any residual data uncertainty. First, in the analysis, the use of dGCPs was restricted to those with a precision within ±0.05 m after post-processing. The position of the continuously recording base was also corrected to better than ±0.05 m. Second, as noted above, bundle adjustment solutions were sought and obtained that were commensurate in terms of their RMSE with the theoretical precision, under the assumption of negligible mean error in the bundle adjustment (Table 1). This suggests that the method will deliver results that are optimal given the image scale and scanning resolution. Third, in the analysis, more GCPs than the minimum necessary were always added to calculate a solution to the bundle adjustment. This allowed comparison of the fitted GCP positions to their field measurements and so calculation of a mean error and a standard deviation of error (σ_i) (Table 1) for each date *i*. In all cases, the mean error was found to be negligible (< 0.05 m) (Table 1). That is, there was no major systematic bias in the solutions. However, this overlooks the fact that the precision of individual data points will not be zero and if the mean error is negligible, it is the point precision that controls the magnitude of change necessary to be deemed significant (Lane *et al.* 2003). Thus, for each pair of datasets being compared, under the assumption that the error is Gaussian, random, and uncorrelated between the pair of datasets being considered, the detectable level of change, with a 95 % confidence, was defined as (Lane *et al*. 2003):

$$\left|dz_{i-1,i}\right| > 1.96 * \left|\sqrt{\sigma_{i-1}^2 + \sigma_i^2}\right| \quad [2]$$

This was used to quantify the magnitudes of change detectable (Table 1) when comparing datasets. It was also used to determine the uncertainty in the volume of change estimates (Table 1) using (Lane *et al.* 2003):

$$\sigma_v = Ar^2 dz_{i-1,i} \qquad [3]$$

with A is the the area used for volume of change computation; and r is the the resolution, in this case 1 m.

Correction of volumes of change for ice mass flux

Volumes of ice mass gain or loss cannot be determined directly from volumes of change without correction for ice mass flux. However, the one-dimensional (1D) mass balance of a glacier can be determined from (Cogley *et al.* 2011):

$$\frac{dV_{ice}}{dt} = \frac{dV}{dt} + A_u\overline{U} \qquad [4]$$

where t is the time: V_{ice} is the the volume of ice mass loss or gain; V is the volume of surface change detected from the DEMs of difference; A_u is the the glacier cross-sectional area across the upstream boundary of the glacier; and $\overline{U}$ is the the section averaged velocity obtained by multiplying the glacier surface velocity in the region of the upstream boundary by 0.9 (following Kääb 2001). Our calculations of flux are across a boundary that is not orthogonal to the downstream direction and so our measures should be seen as flux across this boundary.

The parameter A_u for each date was determined across the upstream section by extracting the altitude along the section from the DEM for each date and combining this with a DEM of the glacier bed provided by Dr. I Willis (Cambridge University) and interpolated from single point radio echo-sounding (Sharp *et al.* 1993). As A_u differs for the start year and the end year, a mean of the results was effectuated between the two years of interest.

To estimate $\overline{U}$, the orthoimages were first used to identify surface displacements from points common to consecutive image pairs. In our application, there was too much image decorrelation with the temporal separation of images to allow application of automated methods (e.g. Scherler *et al.* 2008), and so a manual approach was adopted. A minimum of seven large blocks common to date-sequential pairs of orthoimages were identified and digitised. In order to capture the section-integrated velocity, these were obtained from across the glacier width close to the upstream boundary described above. Identifying more than seven blocks with confidence from across the upstream section was challenging. The mean and standard deviation of block velocity was then calculated between image pairs using the displacement of their *X* and *Y* positions (Table 2), the standard deviation capturing the uncertainty due to cross-valley variation in surface velocity.

Results

Data quality

With reference to Table 1, the global RMSE for image exterior orientation was better than ±0.90 m in all cases and more precisely better than ±0.40 m except for the oldest imagery (1967) that had an RMSE of ±0.59 m, and the imagery with the smallest scale (1988) that had an RMSE of ±0.88 m. Indeed, there is a general positive association between *x* in Table 1 and the global RMSE of the solution. As the focus is on vertical changes of ice mass surfaces that were relatively smooth, the *Z* RMSE is of particular interest. This was better than ±0.09 m except for 1988. The σ_i indicated that the residuals of the control point standard deviation were similar in magnitude to the RMSE *Z* reflecting minimal mean error in the solution. Thus, the level of detection possible was always better than ±1 m. The interpretation of the magnitude of these changes, as well as the volume uncertainty shown in Table 1, depends upon the actual changes measured and this is discussed further below.

Terminus recession and volume loss, 1967-2009

Figure 3 shows glacier stages from 1967. There is a continuous retreat of the glacier snout, with no advance during the cooler periods shown in Figures 1 and 2. The glacier snout also narrows in width. From 1967 to 1988, snout recession was mainly along a West-East line. From 1988 onwards, given the valley morphology, recession was oriented North-North-West to South-South-East and became markedly greater in the middle of the snout than in the partially debris-covered moraines on the glacier margins.

In all periods, volumes of surface change implied volume loss, but with relatively low uncertainty, between one and two orders of magnitude smaller than the actual loss itself (Table 2). When expressed per year, the raw volumes suggested greater loss in two periods: 1977-1983; and 1997-2000. Since the latter period, as the volume of ice in the area of interest as diminished, so has the volume loss, and the period 2005-2009 showed the smallest rate of loss.

Figure 4 shows the cross-sectional area of the glacier and mean glacier thickness along the upstream boundary. Over the period 1967 to 2009, there is a progressive reduction in the upstream boundary area, and this reflects a loss of both width (Figure 3a) and thinning. However, it is not continual, with a slower rate of loss until 1988 (and almost no loss between 1983 and 1988) and more rapid loss from thereon. By 2009, at the upstream cross-section, the glacier had lost about 75 % of its initial thickness in this zone. The presence of slower rates of thinning, notably between 1967 and 1983 probably reflects the slightly cooler temperatures during this period. There is also some divergence between the loss of area and the loss of thickness: for instance, the rate of reduction in thickness falls between 1983 and 1997 and then rises dramatically after 1997. This reflects changes in the balance between reductions in glacier width and reductions in glacier thickness, with a more rapid width loss as compared to thickness loss for the period 1983 to 1997.

Surface velocities, section-averaged velocities and flux across the upstream boundary

Figure 5 shows the section averaged velocity estimated from tracking surface debris blocks. These comprise the combined effects of ice deformation, subglacial sediment deformation and basal sliding (Willis *et al*. 2003). The flow was more rapid between 1967 and 1977. It decreased progressively until 1988 and then remained constant until 1997. The velocity increased between 1997 and 2000. The uncertainty oscillates between 1 % and 22 % of the mean values (Table 2). The flux across the upstream boundary decreases through time despite variability in the section-averaged velocity (Table 2). This reflects progressive thinning of the ice along the upstream boundary.

Volumes of ice mass loss

The volumes of surface change, upstream boundary area and velocity data were combined in [3] to calculate the volumes of ice mass loss (Table 2). The annual melt rate, which is the volume of ice mass loss (m^3y^{-1}) divided by the area (m^2), was also determined (Figure 5). Between 1967 and 1997, the melt rate was relatively constant. The years 1997 to 2000 saw a major increase, with more than 7 $m^3m^{-2}y^{-1}$ of loss. This was lower in 2000-2005 and 2005-2009 but still at a higher level than before 1997, both in absolute terms and also as a proportion of the total ice loss. Glacier thinning, which will reduce the downstream flux, thus contributes to the rapid rate of retreat of the snout.

Comparison with water yield from the basin

The water yield was computed using data from HYDRO Exploitation SA. Table 2 shows a continual increase in yield, with water production at present about 50 % higher than the 1960s. There was no real trend before 1977 and greater variability until 1997. This yield comes from annual snowmelt within the catchment as well as glacier ice melt. It is possible to estimate the relative contribution of these variables by normalizing the volumes by year and comparing them to the volumes of ice mass loss (Table 2). The respective density of water (1000 kgm^{-3}) and an effective density of 850 kgm^{-3} (after Huss 2013) were used for this comparison. The studied part of the glacier has been responsible for c. 2 % to c. 5 % of annual flow. However, it was markedly variable, increasing between 1967 and 1983, being lower up until 1997, reaching a maximum contribution between 1997 and 2000, and then declining progressively until its lower level in 2009.

Discussion

Data quality

The quality of the results depends firstly on the quality of the imagery available. The aerial images have to be cloud free, shadow free on the zones of interest, without snow cover on the glacier and with as large a scale as possible, as scale directly controls the precision of the results obtained. As Table 1 shows, the poorest results were obtained with the smallest scale imagery (note that *x* in Table 1 is the reciprocal of scale). However, as the data in Table 2 showed, this translates into relatively low uncertainties when multi-year comparisons are being made for a system where the changes at the multi-year scale can be large.

To reconstruct the position and orientation of images, ground control points were required. The quality of the result depended on the quality of the individual data points, the density of data points used and their distribution across the surface (Lane *et al*. 2003). In this way, the 20 points selected were recorded with better than ±0.05 m precision to cover as much of the imagery as possible. Nevertheless, some areas were not accessible, such as the western part and the upper part of the glacier because of unstable and difficult terrain. Thus the North-East part, the sandur and the region of the Refuge des Bouquetins were the best identified. This did not lead to an optimal distribution of control points and meant that tie points were critical in improving the solution.

These issues aside, the error analysis still produced encouraging results: the global RMSE was always better than ±0.88 m and better than ±0.45 m for the *Z* co-ordinate. The uncertainties in the volumes of ice mass loss after propagation of error were less than 10 % of the measured volume except for 1988, which had the poorest image scale. These low levels of uncertainty confirm that this method can be used to reconstruct snout recession and surface change of glaciers provided the image scale is sufficient. Moreover, if combined with measurements of surface velocity, it can be used to calculate ice volume changes. Thus, the approach can provide valuable data on glacier response to climate forcing over multiple decades for unmonitored glaciers as well as those where only snout positions are available.

Glacier recession and climate forcing

As shown in Figure 3, the Haut Glacier d'Arolla has been in continuous recession since 1967, despite the snowier and colder periods recorded in Switzerland in the late 1970s and early 1980s during which most Swiss glaciers advanced (Haeberli and Beniston 1998). Its continuous recession, without any noticeable advance since the Little Ice Age, has been noted by others (e.g. Fischer *et al*. 2014).

The annual average melt rate (Figure 5) for the period 1977 to 1983, characteristic of this cooler period (Figure 1, 2b), was actually quite similar to the preceding (1967-1977) and following (1983-1988) warmer periods. The data help to understand why this is the case. In order for the Haut Glacier to advance during the early 1980s, two conditions must be met: (1) the amount of snow and ice accumulation over several years should exceed the amount of ablation (Paterson 1994); and (2) the accumulation, which will tend to be in the upper part of the basin, must be able to translate to the glacier terminus sufficiently rapidly that it can lead to a glacier advance. Thus, whilst the temperature and precipitation conditions between 1977 and 1983 may have combined to create a positive mass balance, for this to translate into a glacier advance, there are two conditions required. The first is an increase in the flux rate from the upper basin accumulation zone, and its translation downstream. The second is a reduction in the snout ablation rate to values lower than the flux rate.

The flux rate is a function of both the cross-section area and the glacier velocity. Cross-section areas progressively reduce through time (Figure 4), so reducing the flux rate to the snout. Glacier surface velocities measured from the orthorectified images were on average *c.* 4 my^{-1} (Figure 5). They can be considered as realistic as they match other scientific research on the Haut Glacier d'Arolla (e.g. Harbor *et al.* 1997: 8 $myear^{-1}$ at the glacier center-line; Hubbard *et al*. 1998: mean of 5 to 6 $myear^{-1}$; Mair *et al*. 2002, 2008). Thus, if the surface velocities measured for the Haut Glacier d'Arolla (Table 2) are representative of the whole glacier, then the glacier equilibrium line altitude will either need to be depressed to very low levels indeed; or the duration of depression must be very long; for an increase in flux arising from upstream accumulation to counter the effects of rapid glacier thinning and snout recession, and for there to be an accumulation-related advance. With the velocities measured, the Haut Glacier d'Arolla is less sensitive to short duration increases in accumulation, and an ablation signal dominates.

The ice flux divergence of a glacier is an important component as it determines the rate of temporal changes of its thickness (Seroussi *et al.* 2011). Taking cross-section area and velocity changes together, for the Haut Glacier d'Arolla, flux was responsible for approximately 35 % of the volume of ice mass lost from the studied area between 1967 and 1977. This decreased to about 15 % between 2005 and 2009. As flux became less important, with climate change (Figures 1, 2b), the thinning glacier was no longer able to sustain its snout position because of falling flux.

It is perhaps surprising given the progressive reduction in ice thickness (Figure 4) that ice velocity (Figure 5) decreases so slowly. Following Cuffey and Paterson (2010) and assuming that the longitudinal stresses (τ_L) are much smaller than the sidewall stresses (τ_w) in this glacier, then (Cuffey and Paterson 2010):

$$\tau_D = \tau_b + \tau_w \qquad [5]$$

where *D* indicates the driving stresses and *b* the basal stresses. This gives a simple model for the cross-section averaged glacier surface velocity (*U*) (Cuffey and Paterson 2010) based upon:

$$\tau_D = \rho g H \alpha$$

$$\tau_b = (\lambda' + c_z H/\eta)^{-1} U$$

$$\tau_w \approx +\eta H U / Y^2 \qquad [6a, 6b, 6c]$$

where: ρ is the density of ice; *g* is the gravity constant; *H* is the mean glacier thickness; α is the glacier surface slope; λ' is a lubrication parameter; c_z is a coefficient related to the shape of the shear profile; and η is the ice viscosity. Thus, whilst thickness decreases should reduce velocity through reduction in the driving stress and increases in the basal stress, it should also increase the sidewall stresses. Width decreases should also reduce velocity through their effect in the sidewall stresses. Between 1967 and 2009, due to thickness changes (Table 2) in the absence of a lubrication effect, the driving stress should halve and the basal stress double, so leading to a substantial velocity reduction. Applying [5] and [6] has some uncertainty, notably in the parameters c_z and η. Here, the parameter c_z is modelled from data provided in Cuffey and Paterson (2010, Table 8.5), which allows for the shape factor to evolve with the width and the thickness of the glacier. On the basis of the known bed geometry (Sharp *et al.* 1993), we determine c_z for a semi-ellipse and rectangle cross-section. The ice viscosity is taken as 1×10^{14} Pa s (e.g. Pelletier *et al.* 2010). We then take the density of ice as 990 kgm^{-3}; *g* as 9.82 ms^{-2}; and the glacier surface slope as measured at 0.08; and apply [5] and [6] assuming no lubrication. Figure 5 confirms that, uncertainties notwithstanding, there should be a progressive decline in surface ice velocity. Comparison with Figure 6 suggests that whilst the modelled velocities, without lubrication, are of the right order of magnitude, they are generally lower. Introduction of lubrication with λ' = 0.000036 reproduces the measured velocity for 1967 (Figure 5), but there is still a rapid decay of the modelled ice surface velocity that is not measured (Figure 6). This suggests that the lubrication effect is not related to increases in the basal shear stress as represented in [6b]. Rather, the velocity is maintained by short periods of acceleration during spring events, as previously measured for the Haut Glacier d'Arolla (e.g. Mair *et al*. 2003; Nienow *et al*. 2005) and related to subglacial hydrological processes. These appear to be able to compensate for the effects of reducing glacier width and thickness upon velocity.

Even though surface velocities did not decrease as rapidly as might be expected, the flux rate progressively falls (Table 2) because of the declining glacier cross-sectional area. The cooler and snowier period of the late 1970s and early 1980s did not translate into a response of the glacier snout most likely because: (1) the duration of this period was too short and/or the equilibrium line insufficiently was depressed for the increasing accumulation to reach the ablation zone, given the relatively low glacier velocities and hence flux rates (cf. Winkler and Nesje, 2009); and (2) the ablation rate in the snout zone was not depressed sufficiently, such that flux to the snout would become greater than the ablation rate and an advance would occur. Following Winkler and Nesje (2009) a reaction to the precipitation-driven increased accumulation is not witnessed because of the magnitude and speed of onset of the temperature-induced increased ablation that followed. The reaction times to precipitation and temperature change are not the same. Given that the flux rate is low, and that it had already diminished during the 1970s (Table 2), it is possible that the precipitation reaction time has become much longer than the temperature reaction time such that the glacier is predominantly temperature forced. More generally, these data emphasise the importance of factoring glacier reaction time (e.g. Purdie *et al.* 2014) into the interpretation of glacier length records and quantifying glacier response during a period when climate change is so rapid that many glaciers may be in a state of disequilibrium with respect to climate (Zekollari and Huybrechts 2015).

Linkages between climate forcing and water yield

The measured water volumes produced by this catchment increased progressively from 1967 to 2009 (Table 2). The contribution of the ice melt for the studied part of the glacier to these volumes has decreased continually with glacier recession. However, it does show how the Haut Glacier d'Arolla is losing its net storage of water as ice and that, considering just part of the glacier, there is a progressive loss of potential water supply.

Conclusions

In this study, aerial imagery was used from 1967 to 2009 to quantify the dynamics of a glacier that is not in the Swiss Glacier Monitoring database (VAW 2013). The work demonstrates the potential of archival digital photogrammetry to reconstruct glacier advance and recession. Provided that certain conditions are met, it is possible to generate data with a very good precision in the vertical and so to detect surface changes of better than ± 0.3 m over quite long time periods. Critical to this success is the availability of historical aerial imagery of the right scale (see [1]), a glacier surface that is not snow covered, and no clouds cover during image acquisition.

Information generated about the position of the glacier snout demonstrated that the Haut Glacier d'Arolla has been in constant recession since 1967 when most Swiss glaciers witnessed small advances during the late 1970s and early 1980s. The primary reason for this was attributed to the relatively low rate of downstream ice mass flux, and associated glacier response time, which meant that whilst there may have been a reduction in the ablation rate during the colder period, the flux did still not exceed the ablation rate, and hence snout advance was prevented. Thus, the study emphasises the dangers of inferring glacier response to climate forcing from measurements of the terminus position only and the importance of using remote sensing methods as an alternative, especially where historical imagery is available.

Data availability

The digital elevation model data used in this study can be downloaded from the website ebibalpin.unil.ch.

Acknowledgements

This study benefited from financial support from the Fondation Herbette and the University of Lausanne. Special thanks go to the Federal Office of Topography Swisstopo for the provision of aerial images, to HYDRO Exploitation SA for the temperatures, precipitations and water flow data, to the Institute of Earth Surface Dynamics (IDYST) of the UNIL for access to the necessary software, and to Mauro Fischer for his comments on earlier parts of the research.

Authors

GABBUD Chrystelle

Institute of Earth Surface Dynamics (IDYST)

University of Lausanne

Quartier Mouline –Geopolis Building – Room 3117

CH – 1015 Lausanne, Switzerland

Chrystelle.gabbud@unil.ch

MICHELETTI Natan

Institute of Earth Surface Dynamics (IDYST)

University of Lausanne

Quartier Mouline – Geopolis Building – Room 3117

CH – 1015 Lausanne, Switzerland

Natan.micheletti@unil.ch

LANE Stuart Nicholas

Institute of Earth Surface Dynamics (IDYST)

University of Lausanne

Quartier Mouline – Geopolis Building – Room 3207

CH – 1015 Lausanne, Switzerland

Stuart.lane@unil.ch

References

Arnold, N., 2005. Investigation the sensitivity of glacier mass-balance/elevation profiles to changing meteorological conditions: Model experiments for Haut Glacier d'Arolla, Valais, Switzerland. *Arctic, Antarctic and Alpine Research, 37*(2), 139-145.

Baltsavias, E., Fayer, E., Bauder, A., Bösch, H. and Pateraki, M., 2001. Digital surface modelling by airborne laser scanning and digital photogrammetry for glacier monitoring. *Photogrammetric Record, 17*(98), 243-273.

Barrand, N., Murray, T., James, T., Barr, S. and Mills, J., 2009. Optimizing photogrammetric DEMs for glacier volume change assessment using laser-scanning derived ground-control points. *Journal of Glaciology, 55*(189), 106-116.

Brecher, H.H., 1986. Surface velocity determination on large polar glaciers by aerial photogrammetry. *Annals of Glaciology*, 8, 22-26.

Brock, B.W., Willis, I.C. and Sharp, M.J., 2000. Measurement and parameterization of albedo variations at Haut Glacier d'Arolla, Switzerland. *Journal of Glaciology, 46*(155), 675-688.

Brock, B.W., Willis, I.C. and Sharp, M.J., 2006. Measurement and parameterization of aerodynamic roughness length variations at Haut Glacier d'Arolla, Switzerland. *Journal of Glaciology, 52*(177), 281-297.

Chandler, J., 1999. Technical communication – Effective application of automated digital photogrammetry for geomorphological research. *Earth Surface Processes and Landforms*, 24, 51-63.

Cogley, J.G., Hock, R., Rasmussen, L.A., Arendt, A.A., Bauder, A., Braithwaite, R.J., Jansson, P., Kaser, G., Möller, M., Nicholson L. and Zemp, M., 2011. *Glossary of glacier mass balance and related terms, IHP-VII Technical documents in hydrology No. 86, IACS, contribution No. 2.* Paris: UNESCO-International Hydrological Programme.

Cuffey, K.M. and Paterson, W.S.B., 2010. *The physics of glaciers – fourth Edition*. Kidlington: Elsevier Science Ltd.

Dadic, R., Mott, R., Lehning, M. and Burlando, P., 2010. Wind influence on snow depth distribution and accumulation over glaciers. *Journal of Geophysical Research*, *115*(F01012), 1-8.

ERDAS, 2009. *LPS Project Manager – User's Guide*. USA: Author.

Finsterwalder, S., 1890. Die Photogrammetrie in den italienischen Hochalpen. *Mittheilungen des Deutschen und Österreichischen Alpenvereins, 16*(1), 6-9.

Fischer, M., Huss, M., Barboux, C. and Hoelzle, M., 2014. The new Swiss Glacier Inventory SGI2010: Relevance of using high-resolution source data on areas dominated by very small glaciers. *Arctic, Antarctic, and Alpine Research,46*(4), 933-945.

Fischer, U., Mair, D., Kavanaugh, J., Willis, I., Nienow, P. and Hubbard, B., 2011. Modelling ice-bed coupling during a glacier speed-up event: Haut Glacier d'Arolla, Switzerland. *Hydrological Processes*, 25, 1361-1372.

Francou, B. and Vincent, C., 2010. *Les glaciers à l'épreuve du climat*. Marseille : Institut de recherche pour le développement, IRD Éditions.

Haeberli, W. and Beniston, M., 1998. Climate change and its impacts on glaciers and permafrost in the Alps. *Ambio*, 27, 258-265.

Harbor, J., Sharp, M., Copland, L., Hubbard, B., Nienow, P. and Mair, D., 1997. Influence of subglacial drainage conditions on the velocity distribution within a glacier cross section. *Geology*, 25, 739-742.

Heid, T. and Kääb, A., 2012. Repeat optical satellite images reveal widespread and long term decrease in land-terminating glacier speeds. *The Cryosphere*, 6, 467-478.

Hooke, R. LeB., 2005. *Principles of glacier mechanics – Second Edition*. Cambridge: Cambridge University Press.

Houghton, J.T., Meiria Filho, L.G., Callander, B.A., Harris, N., Kattenberg, A. and Maskell, K., 1996. *Climate Change 1995: the Science of Climate Change. Published for the Intergovernmental Panel on Climate Change*. Cambridge: University Press.

Hubbard, A., Blatter, H., Nienow, P., Mair, D. and Hubbard, B., 1998. Comparison of a three-dimensional model for glacier flow with field data from Haut Glacier d'Arolla, Switzerland. *Journal of Glaciology, 44*(147), 368-278.

Hubbard, A., Willis, I., Sharp, M., Mair, D., Nienow, P., Hubbard, B. and Blatter, H., 2000. Glacier mass-balance determination by remote sensing and high-resolution modelling. *Journal of Glaciology, 46*(154), 491-498.

Hubbard, B. and Nienow, P., 1997. Alpine subglacial hydrology. *Quaternary Science Reviews,* 16, 939-955.

Huss, M., 2013. Density assumptions for converting geodetic glacier volume change to mass change. *The Cryosphere*, 7, 877–887

Huss, M., Usselmann, S., Farinotti, D. and Bauder, A., 2010. Glacier mass balance in the south-eastern Swiss Alps since 1900 and perspectives for the future. *Erkunde, 64*(2), 119-140.

IPCC, 2008. Intergovernmental Panel on Climate Change Technical Paper VI – French. Chapitre 3 – Relation entre le changement climatique et les ressources en eau : incidences et mesures d'intervention. In B.C. Bates, Z.W. Kundzewicz, S. Wu and J.P. Palutikof (Eds). *Climate Change and Water,* 39-62. Geneva: IPCC Secretariat.

IPCC, 2013. *Climate Change 2013 – The Physical Science Basis*. *Working Group I Contribution to the Fifth Assessment Report of the Intergovernmental Panel on Climate Change – WMA/UNEP*. UK: Cambridge University Press.

Johannesson, T., Raymond, C. and Waddington, E., 1989. Time-scale for adjustment of glaciers to changes in mass balance. *Journal of Glaciology*, 35, 355-369.

Kääb, A., 2001. Photogrammetric reconstruction of glacier mass-balance using a kinematic ice-flux model. A 20-year time-series on Grubengletscher, Swiss Alps. *Annals of Glaciology,* 31, 45-52.

Keutterling, A. and Thomas, A., 2006. Monitoring glacier elevation and volume changes with digital photogrammetry and GIS at Gepatschferner glacier, Austria. *International Journal of Remote Sensing, 27*(19), 4371-4380.

Lane, S.N., Westaway, R.M. and Hicks, D.M., 2003. Estimation of erosion and deposition volumes in a large, gravel-bed, braided river using synoptic remote sensing. *Earth Surfaces Processes and Landforms*, 28, 249-271.

Lane, S.N., Widdison, P.E., Thomas, R.E., Ashworth, P.J., Best, J.L., Lunt, I.A., Smith, G.H.S. and Simpson, C.J., 2010. Quantification of braided river channel change using archival digital image analysis. *Earth Surface Processes and Landforms, 35*(8), 971-985.

Mair, D., Hubbard, B., Nienow, P., Willis, I., Fischer, U.H., 2008. Diurnal fluctuations on glacier ice deformation: Haut Glacier d'Arolla, Switzerland. *Earth Surface Processes and Landforms,* 33, 1272-1284.

Mair, D., Nienow, P., Sharp, M., Wohlleben, T. and Willis, I., 2002. Influence of subglacial drainage system evolution on glacier surface motion: Haut Glacier d'Arolla, Switzerland. *Journal of Geophysical Research, 107*(0), X-1 - X-13.

Mair, D., Willis, I., Fischer, U., Hubbard, B., Nienow, P. and Hubbard, A., 2003. Hydrological controls on patterns of surface, internal and basal motion during three "spring events": Haut Glacier d'Arolla, Switzerland. *Journal of Glaciology, 49*(167), 555-567.

Micheletti, N., Lambiel, C. and Lane, S.N., 2015. Investigating decadal-scale geomorphic dynamics in an alpine mountain setting. *Journal of Geophysical Research: Earth Surface*, 120, 2155-2175.

Nienow, P., Sharp, M. and Willis, I., 1998. Seasonal changes in the morphology of the subglacial drainage system, Haut Glacier d'Arolla, Switzerland. *Earth Surface Processes and Landforms*, 23, 825-843.

Nienow, P.W., Hubbard, A.L., Hubbard, B.L., Chandler, D.M., Mair, D.W.F., Sharp, M.J. and Willis, I.C., 2005. Hydrological controls on diurnal ice flow variability in valley glaciers. *Journal of Geophysical Research*, *110*(F04002), 1-11.

OcCC and Proclim, 2007. *Les changements climatiques et la Suisse en 2050 ; Impacts attendus sur l'environnement, la société et l'économie*. Organe consultatif sur les Changements Climatiques et ProClim, Berne : auteurs.

Oerlemans, J., 2001. *Glaciers and Climate Change*. A.A. Balkema Publishers, Lisse.

OFEV and MétéoSuisse, 2013. *Changements climatiques en Suisse – Indicateurs des causes, des effets et des mesures*. Office Fédéral de l'Environnement et Office Fédéral de Météorologie et de Climatologie, Berne: auteurs.

ONERC, 2008. *Changements climatiques dans les Alpes : Impacts et risques naturels. Rapport technique N°1*. Observation National sur les Effets du Réchauffement Climatique, Paris: auteur.

Paterson, W.S.B., 1994. *The physics of glaciers – Third Edition*. Kidlington: Elsevier Science Ltd.

Pelletier, J.D., Comeau, D., and Kargel, J., 2010. Controls of glacial valley spacing on earth and mars. *Geomorphology*, 116, 189–201.

Pellicciotti, F., Brock, B., Strasser, U., Burlando, P., Funk, M. and Corripio, J., 2005. An enhanced temperature-index glacier melt model including the shortwave radiation balance: development and testing for Haut Glacier d'Arolla, Switzerland. *Journal of Glaciology, 57*(175), 573-587.

Pellikka, P. and Rees, W.G., 2010. *Remote Sensing of glaciers – Techniques for topographic, spatial and thematic mapping of glaciers*. London: Taylor and Francis Group.

Purdie, H., Anderson, B., Chinn, T., Owens, I., Mackintosh, A. and Lawson, W., 2014. Franz Josef and Fox Glaciers, New Zealand: Historic length records. *Global and Planetary Change,* 121, 41-52.

Scherler, D., Leprince, S. and Strecker, M.R., 2008. Glacier-surface velocities in alpine terrain from optical satellite imagery-Accuracy improvement and quality assessment. *Remote Sensing of Environment*, 112, 3806-3819.

Seroussi, H., Morlighem, M., Rignot, E., Larour, E., Audry, D., Ben Dhia, H. and Kristensen, S. S., 2011. Ice flux divergence anomalies in 79north Glacier, Greenland. *Geophysical Research Letters*, *38*(L09501), 1-5.

Sharp, M.J., Richards, K.S., Willis, I.C., Arnold, N.S. and Nienow, P., 1993. Geometry, bed topography and drainage system structure of the Haut Glacier d'Arolla, Switzerland. *Earth Surface Processes and Landforms*, 18, 557-571.

Small, R.J., Beecroft, I.R. and Stirling, D.M., 1984. Rate of deposition on lateral moraine embankments, Glacier de Tsidjiore Nouve, Valais, Switzerland. *Journal of Glaciology, 30*(106), 275-181.

Swift, D.A., Nienow, P.W., Spedding, N. and Hoey, T.B., 2002. Geomorphic implications of subglacial drainage system configuration: rates of basal sediment evacuation controlled by seasonal drainage system evolution. *Sedimentary Geology*, 149, 5-19.

VAW Laboratory of Hydraulics, Hydrology and Glaciology, 2013. *Glaciological reports (1881-2009). The Swiss Glaciers – Yearbooks of the Cryospheric Commission of the Swiss Academy of Sciences (SCNAT) published since 1964*. Zürich: ETH. Available on: http://glaciology.ethz.ch/swiss-glaciers/ (Viewed on the 22.07.2014).

Willis, I., Mair, D., Hubbard, B., Nienow, P., Fischer, U. and Hubbard, A., 2003. Seasonal variations in ice deformation and basal motion across the tongue of Haut Glacier d'Arolla, Switzerland. *Annals of Glaciology*, 36, 157-167.

Winkler, S. and Nesje, A., 2009. Perturbation of climatic response at maritime glaciers? *Erdkunde*, 63, 229-44.

Zekollari, H. and Huybrechts, P., 2015. On the climate-geometry imbalance, response time and volume-area scaling of an alpine glacier: insights from a 3-D flow model applied to Vadret da Morteratsch, Switzerland. *Annals of Glaciology,* 56, 51-62.

Tables

Table 1: Image scale, theoretical precision and the RMSE globally and by co-ordinate of the bundle adjustment. *Also shown is the elevation uncertainty calculated from independent assessment and its propagation into uncertainty of elevation changes and calculated volume estimates (see below)*

Year	Image scale, x (1: *x*)	Theoretical precision (m)	Global RMSE of bundle adjustment (m)	RMSE X (m)	RMSE Y (m)	RMSE Z (m)	Mean error Z (m)	σ_i (m)	$dz_{i-1,i}$ (m)	$\sigma_{v, i-1, i}$ (m^3)
1967	13,700	±0.19	±0.59	±0.83	±0.81	±0.04	0.00	±0.04		
1977	10,000	±0.14	±0.39	±0.21	±0.23	±0.01	0.00	±0.01	±0.082	±54,292
1983	12,000	±0.17	±0.35	±0.18	±0.25	±0.08	0.02	±0.09	±0.177	±95,353
1988	22,200	±0.31	±0.88	±0.42	±0.62	±0.45	0.05	±0.49	±0.981	±440,501
1997	9,000	±0.13	±0.36	±0.53	±0.45	±0.06	0.01	±0.06	±0.973	±325,174
2000	9,000	±0.13	±0.37	±0.39	±0.34	±0.07	0.01	±0.07	±0.190	±43,737
2005	11,900	±0.17	±0.36	±0.33	±0.40	±0.04	0.01	±0.05	±0.172	±31,166
2009	13,000	±0.18	±0.30	±0.34	±0.24	±0.07	0.02	±0.07	±0.163	±21,731

Table 2: Volumes of ice mass loss and water yield. *Volumes of surface loss corrected by the flux and with calculated uncertainty and in comparison with the measured water volume*

Period	Volume of surface loss associated with glacier (m^3year^{-1})	A_u (mean for the period) (m^2)	Profile width (m)	Mean ice thickness for the period along the profile (m)	$\bar{U}$ ($myear^{-1}$)	Flux ($A_u\bar{U}$) (m^3year^{-1})	Volume of ice mass loss (m^3year^{-1})	Measured water volume (m^3year^{-1})	Contribution of ice melt from study area to water yield (%)
1967-1977	743,591 ±54,292	82,664	567	145.79	4.97 ±1.14	410,838 ±94,236	1,154,429 ±108,757	20,432,880	4.80 ±0.46
1977-1983	1,017,378 ±95,353	74,436	541	137.59	4.39 ±0.33	326,772 ±24,564	1,344,150 ±98,466	21,870,150	5.22 ±0.12
1983-1988	747,548 ±440,501	69,331	549	126.29	3.62 ±0.73	250,977 ±50,611	998,525 ±443,399	23,357,340	3.63 ±0.28
1988-1997	596,346 ±325,174	58,757	538	109.21	3.75 ±0.55	220,340 ±32,317	816,686 ±326,776	24,951,300	2.78 ±0.18
1997-2000	1,477,138 ±43,737	42,704	420	101.68	4.61 ±0.63	196,865 ±26,903	1,674,003 ±51,349	26,552,400	5.36 ±0.10
2000-2005	691,250 ±31,166	34,128	402	84.90	4.11 ±0.05	140,267 ±1,706	831,517 ±31,213	27,057,920	2.61 ±0.01
2005-2009	504,120 ±21,731	26,219	447	58.66	3.60 ±0.77	94,387 ±20,188	598,507 ±29,662	27,137,286	1.87 ±0.08

Figure captions

Figure 1: Annual temperatures in Switzerland between 1864 and 2009 in function of the deviation from the reference mean established between 1961 and 1990. *In red, years above this mean; in blue, years below this mean; in black, twenty-years weighted average (low-pass Gaussian filter); the numbers indicate hierarchically the hottest years (MétéoSuisse, 2010. Bulletin climatologique annuel – rétrospective annuelle 2009, available at: http://www.meteosuisse.admin.ch/web/fr/climat/climat_aujourdhui/retrospective_annuelle/flash2009.html (Viewed on the 01.07.2014))*

Figure 2: The snout of the Haut Glacier d'Arolla (2a) with temperature (2b) and precipitation (2c) data *(from Micheletti et al., 2015)*

Figure 3: Haut Glacier d'Arolla stages since 1967. *3a, Zone of interest on the 2009 orthoimage; the red outline represents the relief shaded model determined from the 2009 DEM; 3b, Visualisation of glacier stage superimposed on the 2009 relief shaded model. Also shown is the upstream boundary used in the calculation*

Figure 4: Cross-sectional area across the upstream boundary of the glacier and mean ice thickness across the section at each time period

Figure 5: Mean section averaged velocity and annual melt rate with the 95 % errors bars as uncertainty

Figure 6: Modelled ice surface velocity in response to glacier thinning and narrowing. The error bars show the range of modelled surface velocities with a +10% and -10% change in effective ice viscosity (modelled surface velocity increases with a reduction in effective ice viscosity). Also shown are calculations with lubrication, λ' = 0.000036

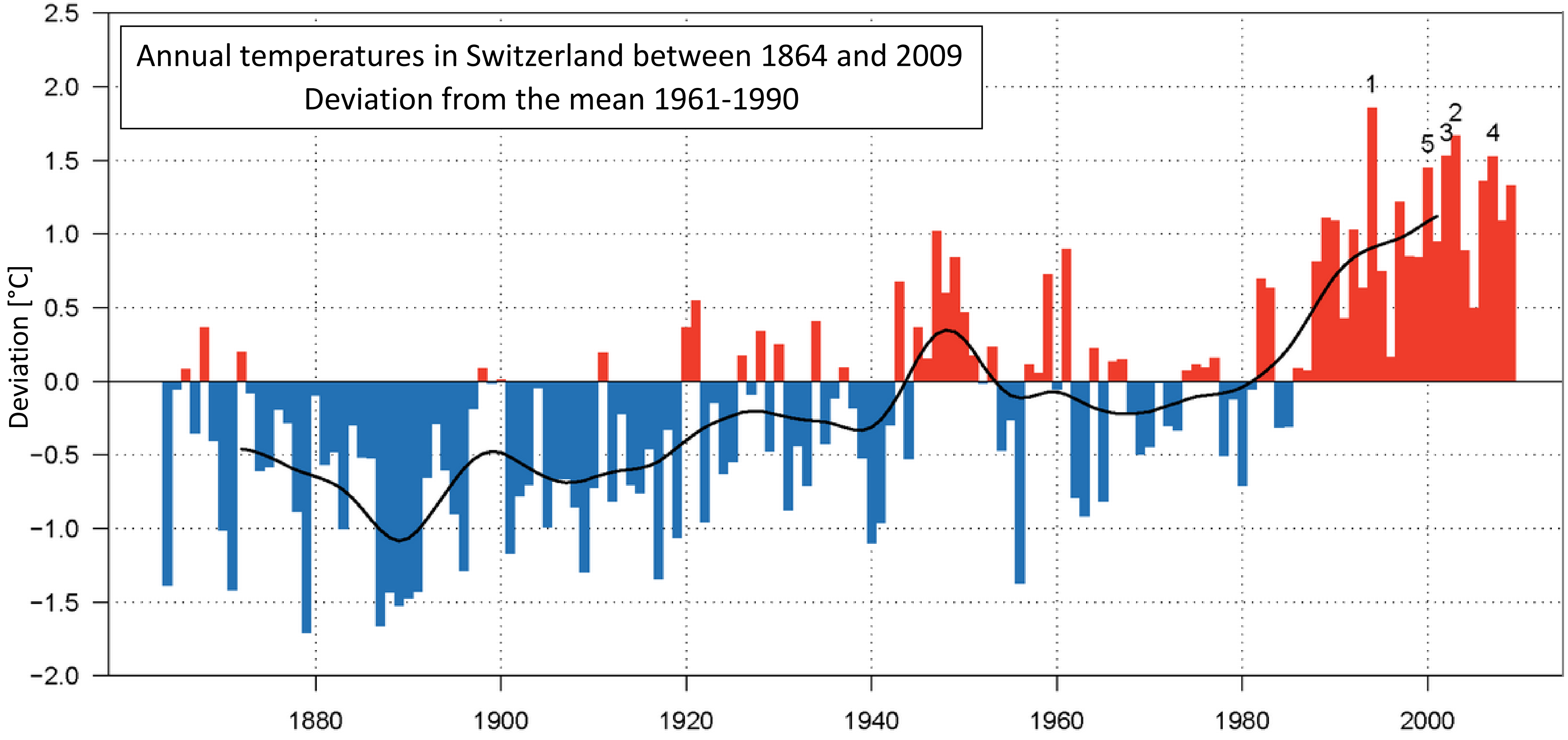
Annual temperatures in Switzerland between 1864 and 2009
Deviation from the mean 1961-1990
Deviation [°C]
2.5
2.0
1.5
1.0
0.5
0.0
−0.5
−1.0
−1.5
−2.0
1880
1900
1920
1940
1960
1980
2000
1
2
3
4
5

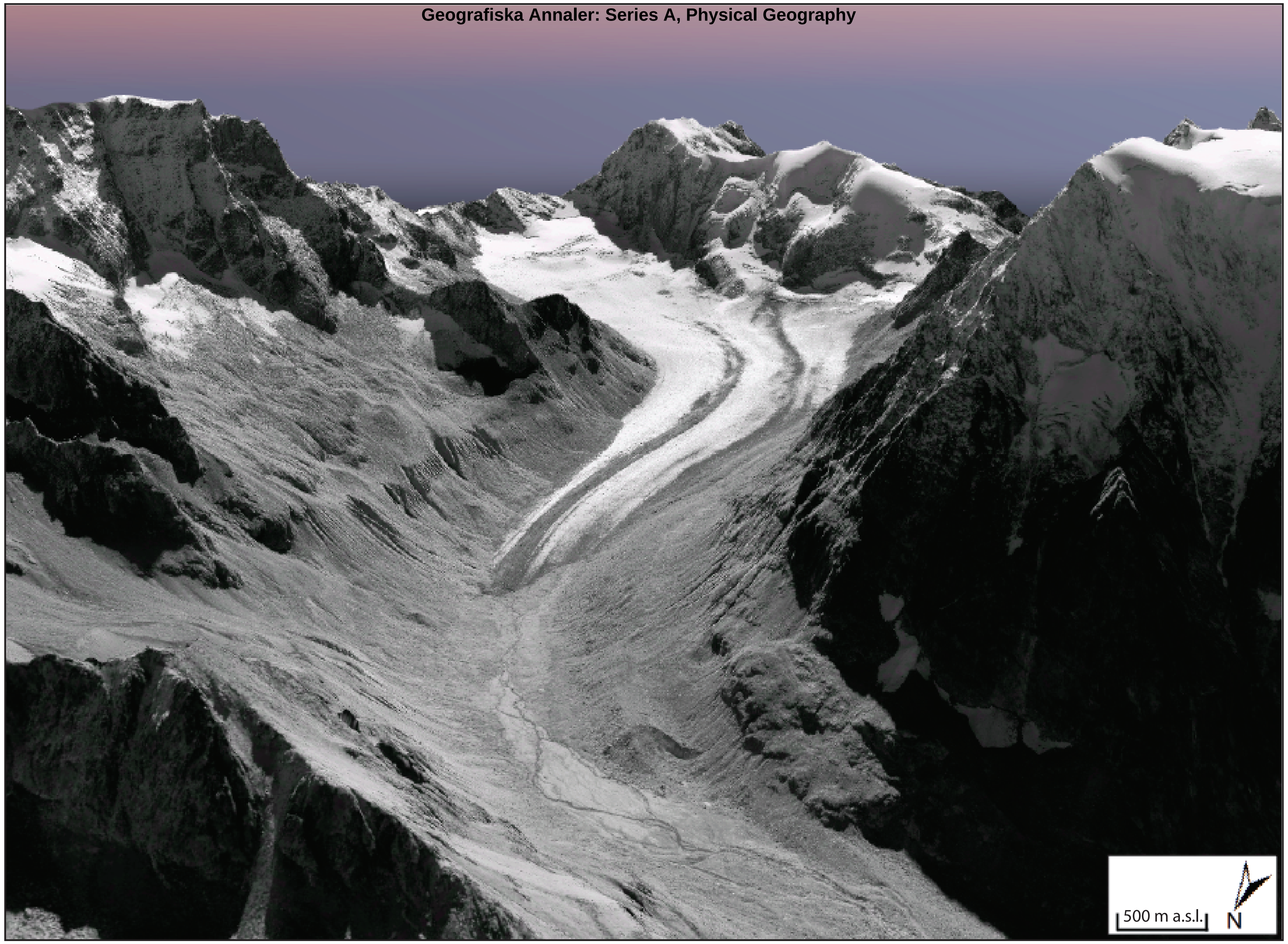
500 m a.s.l.
N

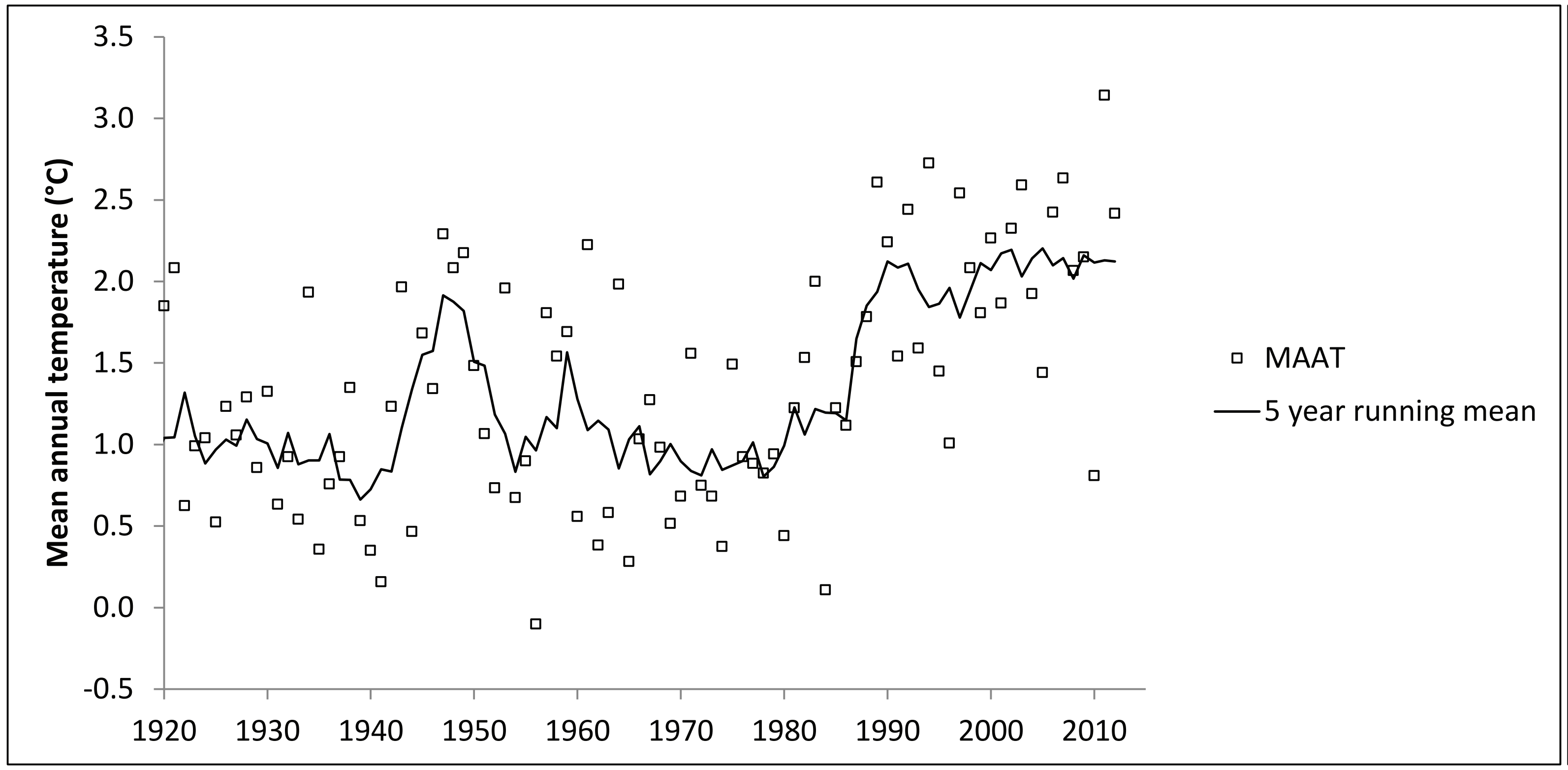
Mean annual temperature (°C)
MAAT
5 year running mean

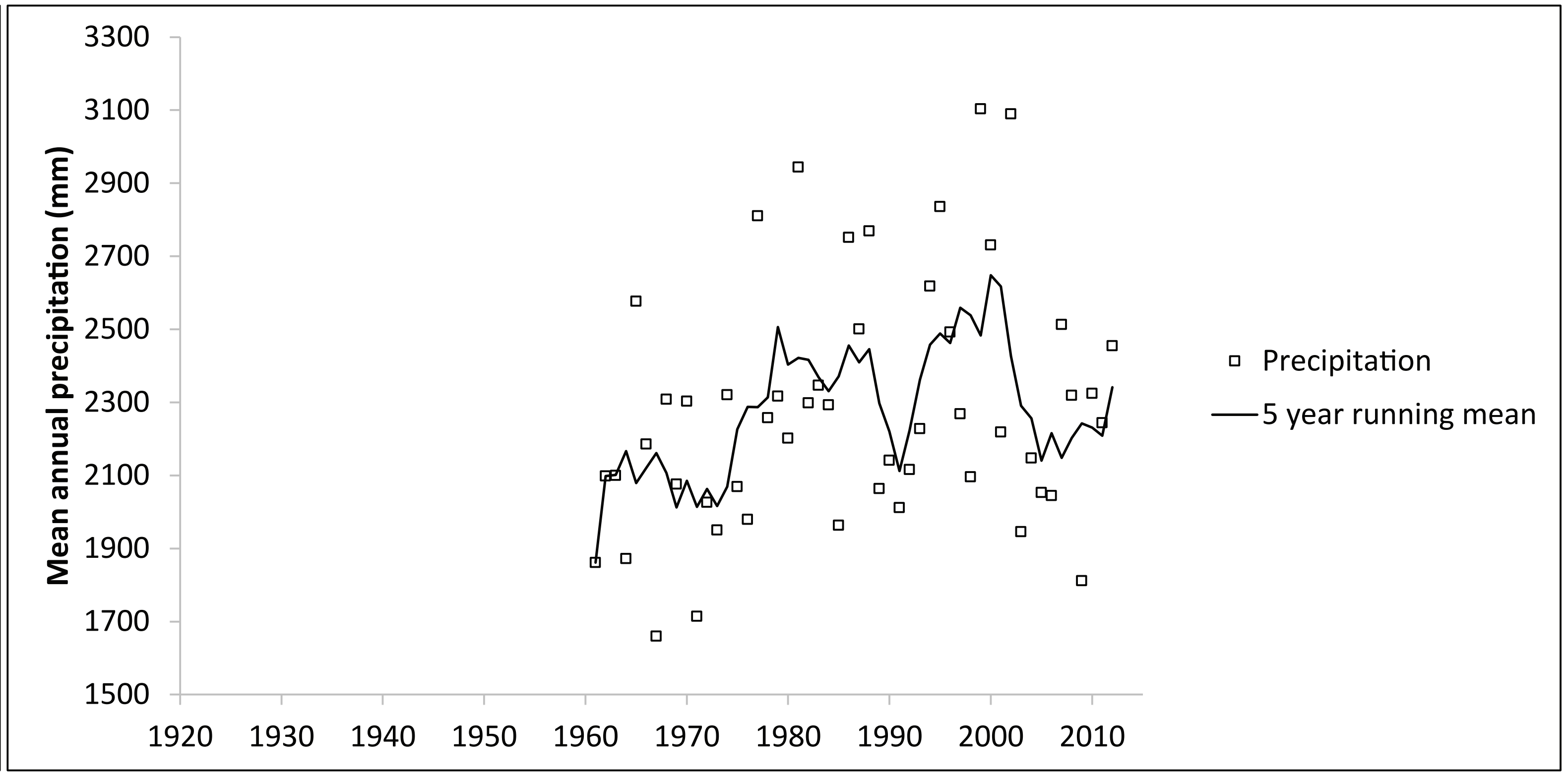
Mean annual precipitation (mm)
Precipitation
5 year running mean

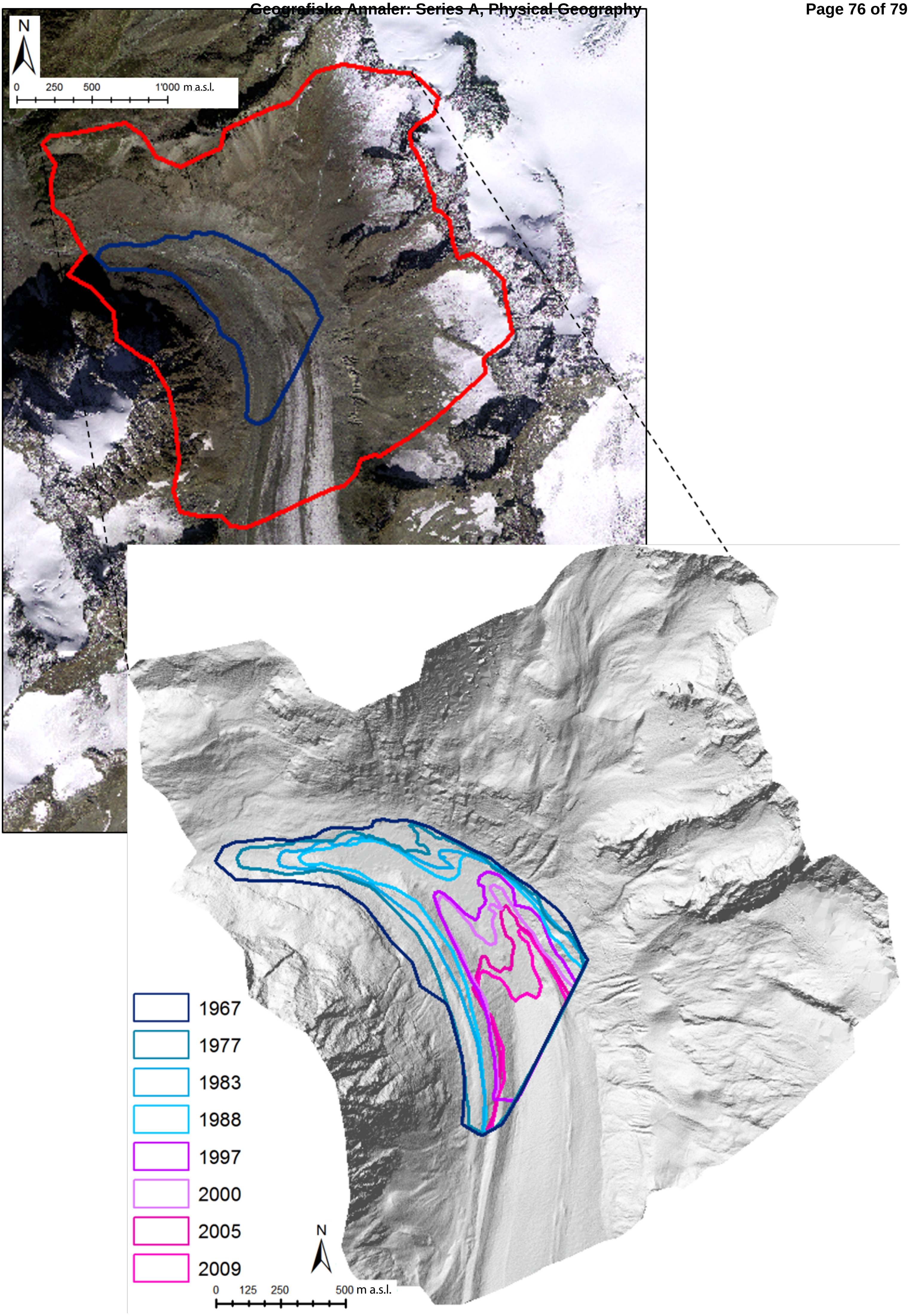
N
0
250
500
1'000 m a.s.l.
1967
1977
1983
1988
1997
2000
2005
2009
N
0
125
250
500 m a.s.l.

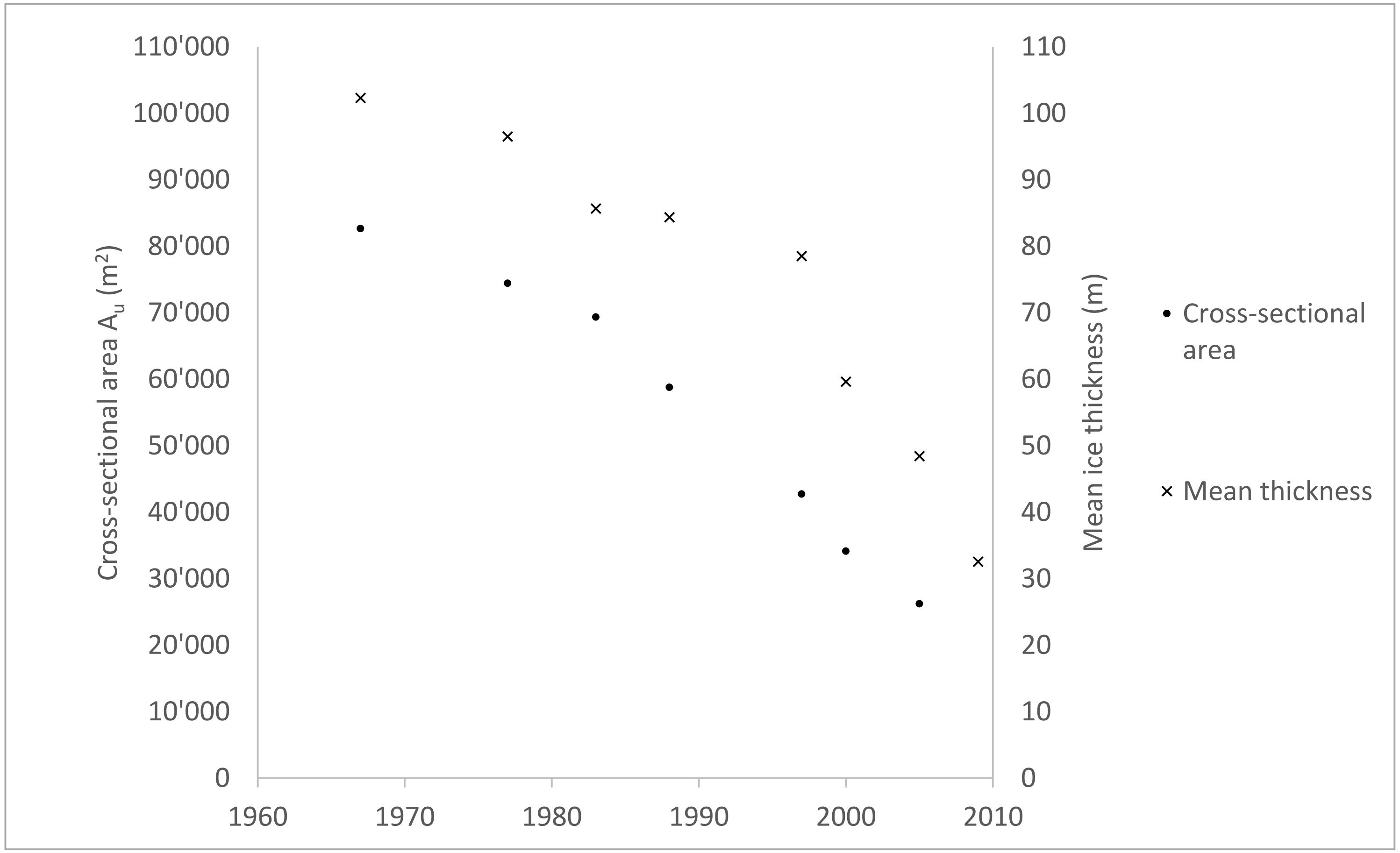

110'000
100'000
90'000
80'000
70'000
60'000
50'000
40'000
30'000
20'000
10'000
0
Cross-sectional area A_u (m^2)
110
100
90
80
70
60
50
40
30
20
10
0
Mean ice thickness (m)
1960
1970
1980
1990
2000
2010
Cross-sectional area
Mean thickness

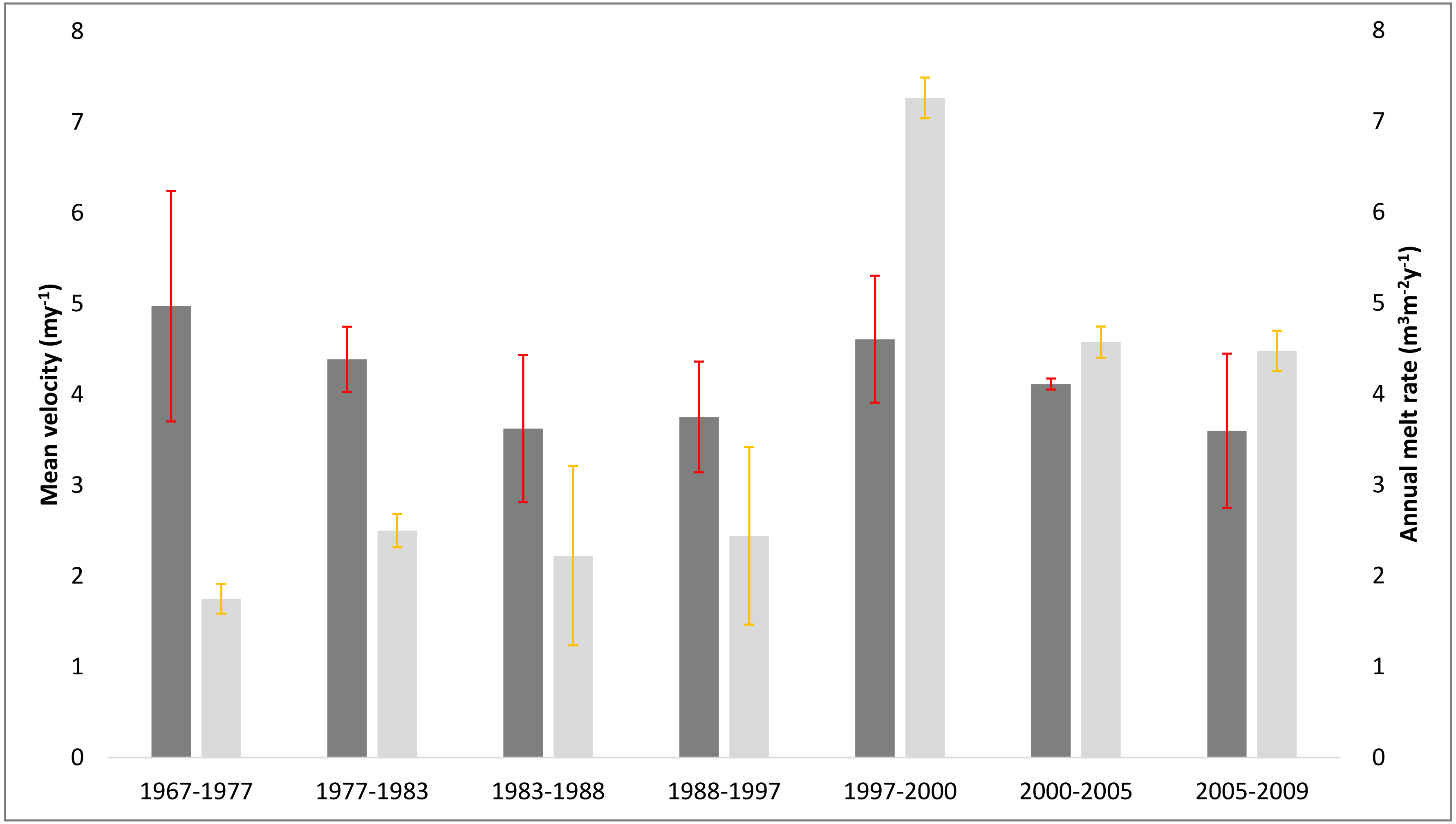
8
7
6
5
4
3
2
1
0
Mean velocity (my-1)
Annual melt rate (m3m-2y-1)
1967-1977
1977-1983
1983-1988
1988-1997
1997-2000
2000-2005
2005-2009

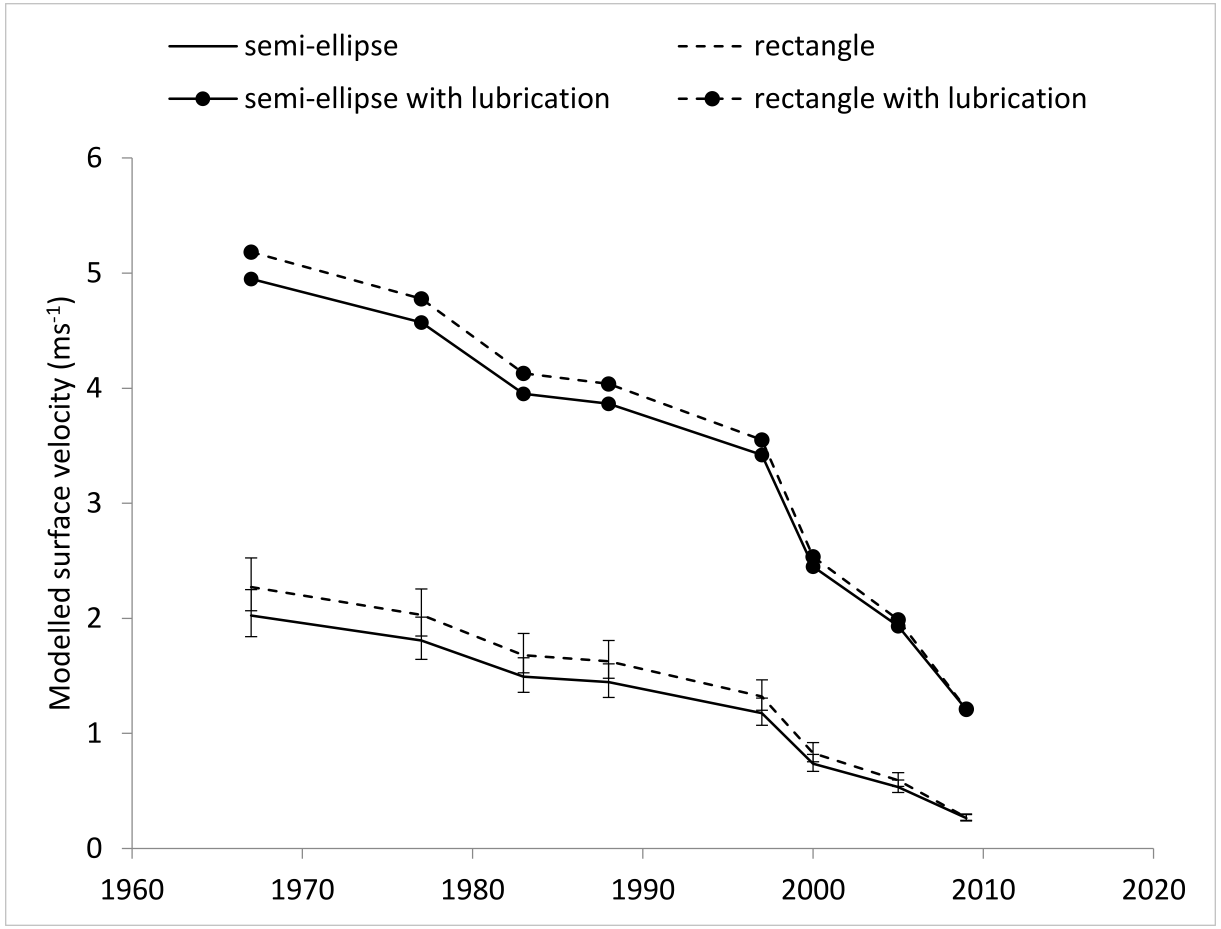
semi-ellipse
rectangle
semi-ellipse with lubrication
rectangle with lubrication
Modelled surface velocity (ms-1)
0
1
2
3
4
5
6
1960
1970
1980
1990
2000
2010
2020